

# Optimal State Feedback Design with Takagi-Sugeno Techniques for the Torque Control of a Nonlinear Hydrostatic Transmission

Harald Aschemann\* and Robert Prabel\*

\*Chair of Mechatronics, University of Rostock, Rostock, Germany

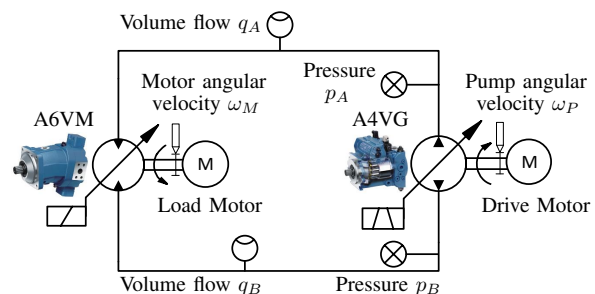
*Summary.* In this paper, a decentralized optimal control approach is proposed for the motor torque provided by a hydrostatic transmission. As basis of the control design, a nonlinear control-oriented model of the hydrostatic transmission is derived. On the one hand, the decentralized structure consists of a flatness-based control of the normalized tilt angle of the hydraulic motor, on the other, of an optimal control design of the hydraulic motor torque based on a Takagi-Sugeno (TS) approach. Given a TS state-space model, the optimal state feedback follows from local optimal designs that are interpolated by exact membership functions. Closed-loop stability is ensured by solving a set of linear matrix inequalities (LMIs) that leads to a joint Lyapunov function. Furthermore, the feedback control is extended by feedforward control to increase the tracking accuracy. An extended Kalman filter estimates the unmeasured states as well as disturbances, which are used for a subsequent disturbance rejection. Finally, the benefits of the proposed control structure are pointed out by simulations using a validated model of a dedicated test rig.

## 1. Introduction

Hydrostatic transmissions (HST), see Figure 1, are usually implemented in construction machines like wheel loaders and



(a) Drive train with a closed-circuit hydrostatic transmission.



(b) Structure of the test rig.

Figure 1: Test rig (a) and structure (b) of a hydrostatic transmission: The dedicated test rig has a closed-circuit structure consisting of an electric drive motor, a hydraulic pump (A4VG), a hydraulic motor (A6VM), an electric load motor, two hydraulic hoses as well as the instrumentation.

excavators as well as in mining and agricultural applications. In the last decade, also in wind turbines, cf. [2, 3, 10], and in power-split gear box systems, cf. [9], the use of hydrostatic transmissions has been considered. In vehicle applications, an internal combustion engine drives the hydraulic pump with a variable volumetric displacement, which is connected to the hydraulic motor by hydraulic hoses in a closed circuit. Given the overpressure between the high-pressure and the low-pressure side, the hydraulic motor, which also offers a variable volumetric displacement, generates a hydraulic torque. Fig. 1 shows a dedicated test rig for the validation of new control concepts, which is available at the Chair of Mechatronics, University of Rostock. Here, two electric motors are used to represent the prime mover as well as to generate specified disturbances, e.g. driving resistance forces.

Concepts for a tracking control of the angular velocity of the hydraulic motor have been presented in previous work, see [12] and [13]. It is also possible, however, to control the hydraulic motor torque that is provided by the hydrostatic transmission to the driven vehicle. An eigenvalue placement based on extended linearisation techniques is presented in [7] in combination with a sliding mode observer. In the given paper, an alternative optimal design of a nonlinear control structure is proposed.

The outline of this paper is as follows: A control-oriented overall system model is developed in Sect. 2. Next, decentralized tracking controllers are derived in Sect. 3 for the motor tilt angle on the one hand, and for the motor torque on the other. In Sect. 4, an extended Kalman Filter is presented that estimates unmeasured state variables – the tilt angles of the hydraulic pump and motor – as well as disturbances – a resulting leakage flow and a load torque. The disturbance estimation and the tracking performance of the overall control structure are investigated in simulations using a validated system model, see Sect. 5. In Sect. 6, the paper finishes with conclusions.

## 2. Mechatronic Model of the Hydrostatic Transmission

A control-oriented model of the hydrostatic transmission provides the necessary information for the control design. Suitable models for hydraulic applications can be found in [6]. The mathematical description of the test rig shown in Fig. 1 can be divided in hydraulic and mechanical subsystems.

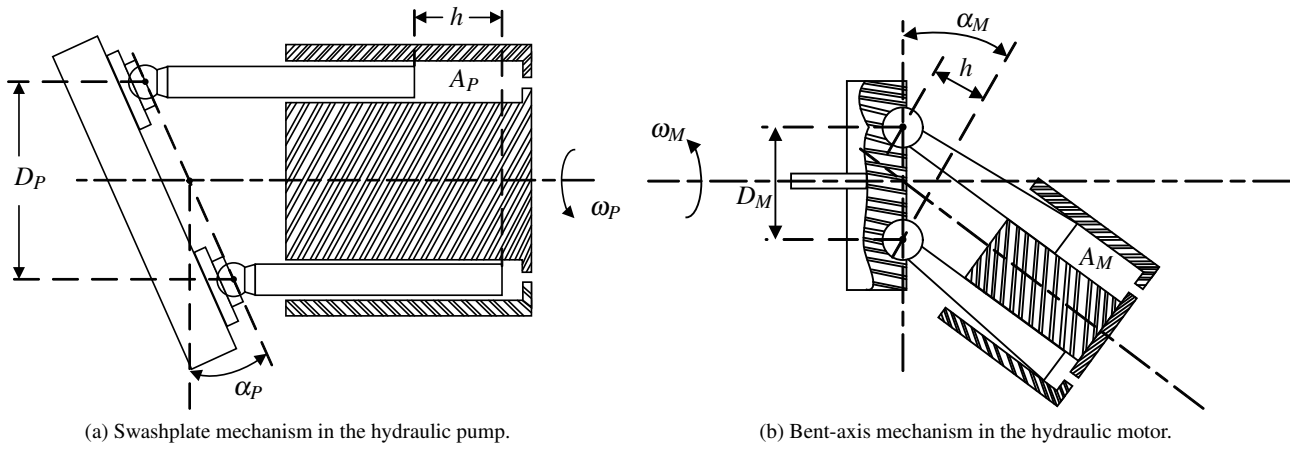


Figure 2: Sketches of the hydraulic pump and the hydraulic motor.

## 2.1 Hydraulic Subsystem

The hydraulic subsystem includes the hydraulic pump – driven by an electric drive motor with underlying velocity control – and the hydraulic motor as well as the pressure dynamics in the hydraulic hoses. The corresponding models for the individual hydraulic components are described in the sequel.

### Pump Flow Rate

The pump ideal flow rate  $q_P$  is determined by a nonlinear function

$$q_P = V_P(\alpha_P) \frac{\omega_P}{2\pi}, \quad (1)$$

with  $\omega_P$  as the angular velocity of the pump. The nonlinear behaviour of the volumetric displacement  $V_P(\alpha_P)$  is related to the mechanical design based on a tiltable swashplate. A mathematical description according to Fig. 2a leads to

$$V_P(\alpha_P) = N_P A_P D_P \tan(\alpha_{P,\max} \cdot \tilde{\alpha}_P), \quad (2)$$

with the normalized swashplate angle  $\tilde{\alpha}_P = \alpha_P / \alpha_{P,\max}$ . The geometrical parameters are the effective piston area  $A_P$ , the diameter  $D_P$  of the piston circle and the number  $N_P$  of pistons inside the pump. The overall pump flow can be described by

$$q_P = \underbrace{\frac{N_P A_P D_P}{2\pi}}_{\tilde{V}_P} \tan(\alpha_{P,\max} \cdot \tilde{\alpha}_P) \omega_P = \tilde{V}_P \tan(\alpha_{P,\max} \cdot \tilde{\alpha}_P) \omega_P. \quad (3)$$

### Motor Flow Rate

The used hydraulic motor is of a bent-axis design, see Fig. 2b. Therefore, the ideal volume flow rate  $q_M$  into the hydraulic motor can be described by

$$q_M = V_M(\alpha_M) \frac{\omega_M}{2\pi}, \quad (4)$$

similarly to the pump. In (4),  $V_M(\alpha_M)$  represents the nonlinear volumetric displacement of the motor and  $\omega_M$  the angular velocity of the motor. With the geometrical parameters  $N_M$ ,  $A_M$  and  $D_M$  of the hydraulic motor, the volume flow rate can be stated as

$$q_M = \underbrace{\frac{N_M A_M D_M}{2\pi}}_{\tilde{V}_M} \sin(\alpha_{M,\max} \cdot \tilde{\alpha}_M) \omega_M = \tilde{V}_M \sin(\alpha_{M,\max} \cdot \tilde{\alpha}_M) \omega_M. \quad (5)$$

Likewise to the mathematical description of the flow rate of the pump, a normalized bent-axis angle is introduced with  $\tilde{\alpha}_M = \alpha_M / \alpha_{M,\max}$ .

### Pressure Dynamics

The pressure dynamics of the high-pressure and the low-pressure sides of the hydrostatic transmission are given by

$$\dot{p}_A = \frac{\beta_A}{V_A} (q_P - q_M - q_I - q_{E,A}) \quad \text{and} \quad \dot{p}_B = \frac{\beta_B}{V_B} (-q_P + q_M + q_I - q_{E,B}), \quad (6)$$

with the effective bulk moduli  $\beta_k$ ,  $k \in \{A, B\}$  and the total compression volumes  $V_k$ ,  $k \in \{A, B\}$ , which take into account the hydraulic hoses and the chambers, respectively. The volume flow balances for the compression volumes depend on

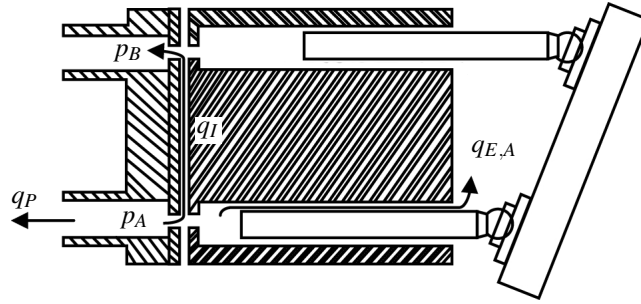


Figure 3: Example for the leakage paths for a axial piston hydraulic pump, with the internal leakage  $q_I$  and the external leakage  $q_E$ .

the volume flows  $q_i$ ,  $i \in \{P, M\}$  of the pump and the motor, an internal leakage flow  $q_I$  as well as external leakage flows  $q_{E,k}$ ,  $k \in \{A, B\}$ , see Fig. 3. Next, a symmetric set-up regarding the high- and low-pressure sides is assumed. The hydraulic capacity with  $C_H = V/\beta$  can be considered as nearly identical with  $C_A = C_B =: C_H$ . To reduce the model complexity for the control design, the difference pressure  $\Delta p = p_A - p_B$  is introduced. The corresponding differential equation is given by

$$\Delta \dot{p} = \frac{2}{C_H} (\bar{V}_P \tan(\alpha_{P,\max} \cdot \tilde{\alpha}_P) \omega_P - \bar{V}_M \sin(\alpha_{M,\max} \cdot \tilde{\alpha}_M) \omega_M) - \frac{q_u}{C_H}, \quad (7)$$

where

$$q_u = 2q_I + q_{E,A} - q_{E,B} \quad (8)$$

represents a resulting leakage oil flow acting as a disturbance.

### Actuator Dynamics

It is obvious that an instantaneous change of the displacement of the hydraulic pump as well of the hydraulic motor is impossible. To model such a lag behaviour, first-order lag models are introduced according to

$$T_{uP} \dot{\tilde{\alpha}}_P + \tilde{\alpha}_P = k_P u_P \quad \text{and} \quad T_{uM} \dot{\tilde{\alpha}}_M + \tilde{\alpha}_M = k_M u_M. \quad (9)$$

Here,  $T_{uP}$  and  $T_{uM}$  represents the corresponding time constants,  $k_P$  and  $k_M$  the proportional gains and  $u_P$  and  $u_M$  the analogue input voltages of the servo valves. Furthermore, the angles are bounded due to the mechanical design with  $\tilde{\alpha}_P \in \{-1, 1\}$  and  $\tilde{\alpha}_M \in \{\varepsilon_M, 1\}$ ,  $\varepsilon_M > 0$ .

### 2.2 Mechanical Subsystem

Typically, hydrostatic transmissions are used in construction machines. In the laboratory environment, see Fig. 1b, the hydraulic motor is connected to an electric load motor, which serves for providing specified driving resistances. The set

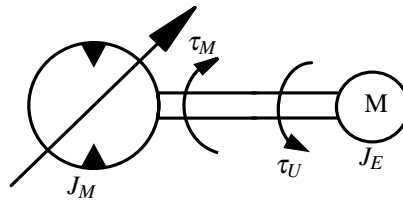


Figure 4: Kinematic structure of the drive train.

up of the remaining drive train of the test rig is depicted in Fig. 4. A torque balance leads to the equation of motion for the hydraulic pump shaft

$$J_V \dot{\omega}_M + d_V \omega_M = \tau_M - \tau_U, \quad (10)$$

with the damping coefficient  $d_V$  and  $J_V = J_M + J_E$  as the sum of the mass moments of inertia of the hydraulic motor and the electric load motor, which are rigidly connected. Unmodelled disturbances and parameter uncertainties are combined in a lumped disturbance torque  $\tau_U$ . The hydraulic torque of the motor is given by

$$\tau_M = \bar{V}_M \Delta p \sin(\alpha_{M,\max} \cdot \tilde{\alpha}_M). \quad (11)$$

### 2.3 Simulation Model of the Overall System

The dynamics of the test rig can be characterized by four first-order differential equations. By introducing the normalized tilt angles  $\tilde{\alpha}_P$  and  $\tilde{\alpha}_M$ , the difference pressure  $\Delta p$  and the angular velocity of the drive shaft  $\omega_M$  as state variables, the state vector becomes

$$\mathbf{x}_S = \begin{bmatrix} \tilde{\alpha}_P & \tilde{\alpha}_M & \Delta p & \omega_M \end{bmatrix}^T, \quad (12)$$

and the corresponding nonlinear state-space representation results in

$$\underbrace{\begin{bmatrix} \dot{\tilde{\alpha}}_P \\ \dot{\tilde{\alpha}}_M \\ \Delta \dot{p} \\ \dot{\omega}_M \end{bmatrix}}_{\dot{\mathbf{x}}_S} = \underbrace{\begin{bmatrix} -\frac{1}{T_{uP}} \tilde{\alpha}_P + \frac{k_P}{T_{uP}} u_P \\ -\frac{1}{T_{uM}} \tilde{\alpha}_M + \frac{k_M}{T_{uM}} u_M \\ \left[ \frac{2}{C_H} \bar{V}_P \tan(\alpha_{P,\max} \cdot \tilde{\alpha}_P) \omega_P - \frac{2}{C_H} \bar{V}_M \sin(\alpha_{M,\max} \cdot \tilde{\alpha}_M) \omega_M - \frac{q_U}{C_H} \right] \\ -\frac{d_V}{J_V} \omega_M + \frac{\bar{V}_M}{J_V} \sin(\alpha_{M,\max} \cdot \tilde{\alpha}_M) \Delta p - \frac{\tau_U}{J_V} \end{bmatrix}}_{f(\mathbf{x}_S, \mathbf{u}, \tau_U, q_U)}. \quad (13)$$

The input voltages

$$\mathbf{u} = [u_P \ u_M]^T \quad (14)$$

of the proportional valves for the actuation of the hydraulic pump and motor are used as control inputs.

### 3. Nonlinear Tracking Control Design

The proposed control structure is based on a decentralized approach. In a first control loop, the normalized tilt angle of the hydraulic motor  $\tilde{\alpha}_M$  is controlled by a flatness-based approach. The second control loop is responsible for the torque control of the hydraulic motor and uses Takagi-Sugeno (TS) techniques for the feedback control design, which enable a stability proof by LMIs.

#### 3.1 Flatness-Based Control of the Tilt Angle of the Hydraulic Motor

The control design for  $\tilde{\alpha}_M$  is performed using a flatness-based approach, see [4]. Thereby, the inverse dynamics results in

$$u_M = \frac{\tilde{\alpha}_M + v_M T_{uM}}{k_M}, \quad (15)$$

with the stabilising control law

$$v_M = \ddot{\tilde{\alpha}}_{Md} + k_{\alpha 0} e_{\tilde{\alpha}_M} + k_{\alpha I} \cdot \int_0^t e_{\tilde{\alpha}_M} d\tau. \quad (16)$$

Here,  $e_{\tilde{\alpha}_M} = \tilde{\alpha}_{M,d} - \tilde{\alpha}_M$  represents the tracking error of the normalized tilt angle. The second-order error dynamics regarding  $e_{\tilde{\alpha}_M}$  is parametrized with positive coefficients  $k_{\alpha 0} > 0$  and  $k_{\alpha I} > 0$ . The integrator part in (16) counteracts uncertainty in the actuator dynamics and leads to steady-state accuracy.

#### 3.2 Tracking Control Design for the Motor Torque

Linear control approaches like eigenvalue placement and LQR design are well known and often used for linear state-space systems. These designs can be extended to nonlinear systems using either extended linearisation techniques as in [5, 2] or Takagi-Sugeno (TS) techniques, see [14, 9, 10]. This paper employs TS techniques for the optimal nonlinear control design, whereas an eigenvalue placement with extended linearisation is investigated in [7]. To derive an exact TS representation, cf. [14], the system is written in quasi-linear form as follows

$$\begin{aligned} \dot{\mathbf{x}}(t) &= \mathbf{A}(\tilde{\alpha}_P, \omega_P) \mathbf{x}(t) + \mathbf{b} u(t) + \mathbf{e} z(t), \\ y(t) &= \mathbf{c}^T(\tilde{\alpha}_M) \mathbf{x}(t). \end{aligned} \quad (17)$$

In detail, the quasi-linear form can be stated as

$$\dot{\mathbf{x}} = \underbrace{\begin{bmatrix} \frac{-1}{T_{uP}} & 0 \\ \frac{2 \bar{V}_P \omega_P \operatorname{sinc}(\alpha_{P,\max} \cdot \tilde{\alpha}_P) \cdot \alpha_{P,\max}}{C_H} & 0 \end{bmatrix}}_{\mathbf{A}(\tilde{\alpha}_P, \omega_P)} \underbrace{\begin{bmatrix} \tilde{\alpha}_P \\ \Delta p \end{bmatrix}}_{\mathbf{x}} + \underbrace{\begin{bmatrix} \frac{k_P}{T_{uP}} \\ 0 \end{bmatrix}}_{\mathbf{b}} u_P + \underbrace{\begin{bmatrix} 0 \\ \frac{1}{C_H} \end{bmatrix}}_{\mathbf{e}} \underbrace{-2 \bar{V}_M \omega_M \sin(\alpha_{M,\max} \cdot \tilde{\alpha}_M) - q_U}_{z}. \quad (18)$$

The system matrix  $\mathbf{A} = \mathbf{A}(\tilde{\alpha}_P, \omega_P)$  depends on the state variable  $\tilde{\alpha}_P$  and on the varying angular velocity  $\omega_P$  of the hydraulic pump, whereas the vectors  $\mathbf{b}$  and  $\mathbf{e}$  are constant. The sinc function is determined by  $\operatorname{sinc}(\alpha_P) = \sin(\alpha_P)/\alpha_P$ , with  $\operatorname{sinc}(\alpha_P = 0) = 1$ . The nonlinear output equation results in

$$y = \tau_M = \underbrace{\begin{bmatrix} 0 & \bar{V}_M \sin(\alpha_{M,\max} \cdot \tilde{\alpha}_M) \end{bmatrix}}_{\mathbf{c}^T(\tilde{\alpha}_M)} \mathbf{x}, \quad (19)$$

where the output vector  $\mathbf{c}^T = \mathbf{c}^T(\tilde{\alpha}_M)$  is affected by the tilt angle of the hydraulic motor. Note that for the corresponding feedforward control design  $\tilde{\alpha}_M$  can be considered as a gain-scheduling parameter.

### Controllability Analysis

A subsequent controllability analysis becomes possible with Kalman's controllability criterion

$$\mathbf{Q}_C(\tilde{\alpha}_p, \omega_p) = \left[ \mathbf{b} \mathbf{A}(\tilde{\alpha}_p, \omega_p) \mathbf{b} \right], \quad \det(\mathbf{Q}_C(\tilde{\alpha}_p, \omega_p)) \neq 0, \quad (20)$$

which must be fulfilled for all states  $\tilde{\alpha}_p$  and all angular velocities  $\omega_p$  within the operating range. It turns out that a positive angular velocity  $\omega_p > 0$  guarantees a positive determinant value and, hence, complete controllability. The tilt angle of the motor is confined to strictly positive values  $\tilde{\alpha}_M \in \{\varepsilon_M, 1\}$ ,  $\varepsilon_M > 0$ .

### Optimal Feedback Control Design Using TS Techniques

Based on an exact TS representation of (18), an optimal parallel distributed parallel compensator (DPC) is designed, cf. [14], which results in a state- and parameter-dependent feedback gain vector  $\mathbf{k}^T(\tilde{\alpha}_p, \omega_p)$ . The quasi-linear dynamical system (18) to be stabilized is characterized by a variable system matrix  $\mathbf{A} = \mathbf{A}(\tilde{\alpha}_p, \omega_p)$  and a constant input vector  $\mathbf{b}$ . Discarding the disturbance  $z$  for the feedback control design, the quasi-linear model (18) can be rewritten as

$$\dot{\mathbf{x}} = \underbrace{\begin{bmatrix} \frac{-1}{T_{uP}} & 0 \\ a_{21}(\tilde{\alpha}_p, \omega_p) & 0 \end{bmatrix}}_{\mathbf{A}(\tilde{\alpha}_p, \omega_p)} \underbrace{\begin{bmatrix} \tilde{\alpha}_p \\ \Delta p \end{bmatrix}}_{\mathbf{x}} + \underbrace{\begin{bmatrix} \frac{k_P}{T_{uP}} \\ 0 \end{bmatrix}}_{\mathbf{b}} u_{FB}, \quad (21)$$

where the state- and parameter-dependency of the system matrix is due to the nonlinear function

$$a_{21}(\tilde{\alpha}_p, \omega_p) = \frac{2 \bar{V}_p \omega_p \operatorname{sinc}(\alpha_{p,\max} \cdot \tilde{\alpha}_p) \cdot \alpha_{p,\max}}{C_H \cos(\alpha_{p,\max} \cdot \tilde{\alpha}_p)}. \quad (22)$$

Given the maximum value as well as the minimum value of  $a_{21}(\tilde{\alpha}_p, \omega_p)$ , an exact interpolation becomes possible if the following weighting functions are introduced

$$a_{21}(\tilde{\alpha}_p, \omega_p) = a_{21,\max} \cdot \underbrace{\frac{a_{21}(\tilde{\alpha}_p, \omega_p) - a_{21,\min}}{a_{21,\max} - a_{21,\min}}}_{w_{11}(\tilde{\alpha}_p, \omega_p)} + a_{21,\min} \cdot \underbrace{\frac{a_{21,\max} - a_{21}(\tilde{\alpha}_p, \omega_p)}{a_{21,\max} - a_{21,\min}}}_{w_{12}(\tilde{\alpha}_p, \omega_p)}. \quad (23)$$

With these weighting functions, two different membership functions  $h_l(\tilde{\alpha}_p, \omega_p)$ ,  $0 \leq h_l(\tilde{\alpha}_p, \omega_p) \leq 1$ ,  $l \in \{1, 2\}$ , can be defined according to

$$h_1(\tilde{\alpha}_p, \omega_p) = w_{11}(\tilde{\alpha}_p, \omega_p), \quad h_2(\tilde{\alpha}_p, \omega_p) = w_{12}(\tilde{\alpha}_p, \omega_p), \quad h_1(\tilde{\alpha}_p, \omega_p) + h_2(\tilde{\alpha}_p, \omega_p) = 1, \quad (24)$$

which represent the individual contributions of two corresponding corner models

$$\mathbf{A}_1 = \begin{bmatrix} \frac{-1}{T_{uP}} & 0 \\ a_{21,\max} & 0 \end{bmatrix}, \quad \mathbf{A}_2 = \begin{bmatrix} \frac{-1}{T_{uP}} & 0 \\ a_{21,\min} & 0 \end{bmatrix}, \quad (25)$$

in the polytopic representation

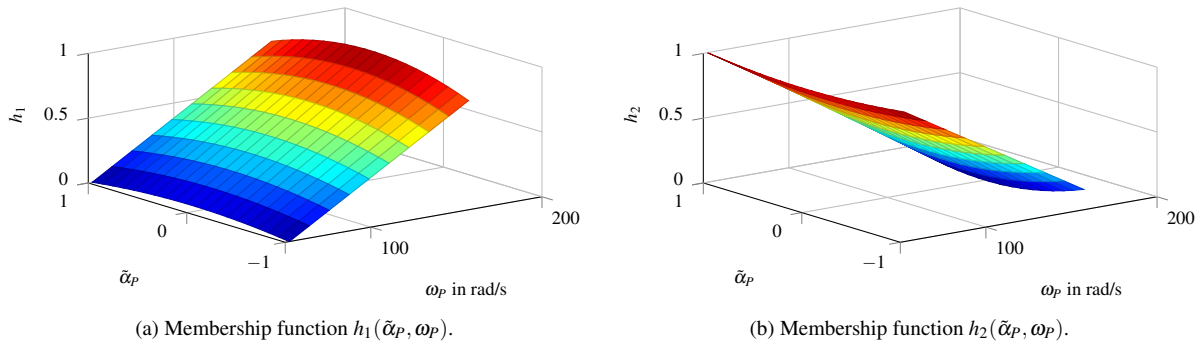
$$\mathbf{A}(\tilde{\alpha}_p, \omega_p) = \sum_{l=1}^2 h_l(\tilde{\alpha}_p, \omega_p) \mathbf{A}_l. \quad (26)$$

The exact membership functions, which correspond to the sector nonlinearity approach in [14], are depicted in Fig. 5. The local design of the state feedback for the each corner model is performed with the linear quadratic regulator (LQR) approach. Here, the vector of feedback gains follows from a minimization of a quadratic cost function with a combined weighting of the state variables as well as the control inputs. The cost function is given by

$$J = \frac{1}{2} \int_0^{\infty} [\mathbf{x}^T \mathbf{Q} \mathbf{x} + r u^2] dt, \quad (27)$$

where the weighting matrix for the state vector  $\mathbf{x}$  is chosen as a positive definite diagonal matrix  $\mathbf{Q} > 0$ , the scalar input weight as a constant positive value  $r > 0$ . For each corner model of the polytope, the optimal feedback control law can be determined as the positive definite, symmetric solution  $\mathbf{P}_l = \mathbf{P}_l^T > 0$  of the algebraic Riccati equation (ARE)

$$\mathbf{A}_l^T \mathbf{P}_l + \mathbf{P}_l \mathbf{A}_l - r^{-1} \mathbf{P}_l \mathbf{b} \mathbf{b}^T \mathbf{P}_l + \mathbf{Q} = \mathbf{0}, \quad l \in \{1, 2\}. \quad (28)$$


 Figure 5: Membership functions  $\underline{h}_l(\tilde{\alpha}_P, \omega_P)$ .

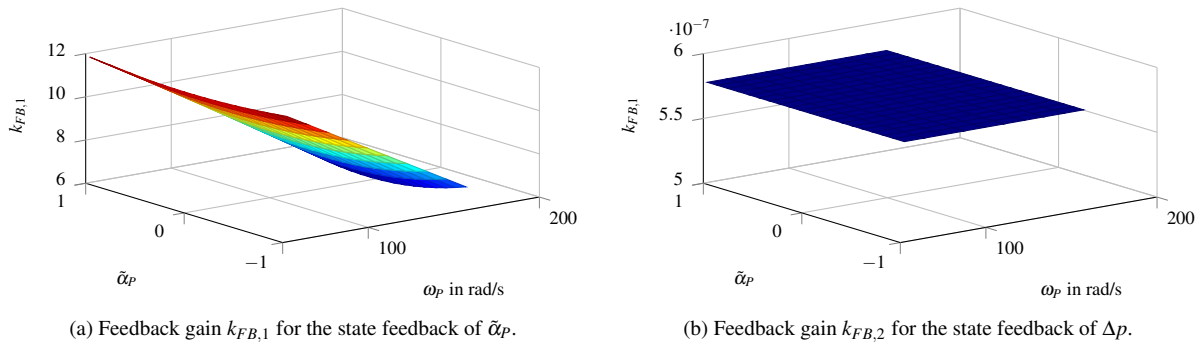
The local state feedback laws for the corner models become

$$u_{FB,l}(\mathbf{x}) = -\mathbf{k}_l^T \mathbf{x} = -r^{-1} \mathbf{b}^T \mathbf{P}_l \mathbf{x}. \quad (29)$$

The overall feedback control law is obtained by the weighted combination

$$u_{FB}(\mathbf{x}, \omega_P) = \sum_{l=1}^2 h_l(\tilde{\alpha}_P, \omega_P) u_{FB,l}(\mathbf{x}) = - \underbrace{\sum_{l=1}^2 h_l(\tilde{\alpha}_P, \omega_P) \mathbf{k}_l^T}_{\mathbf{k}^T(\tilde{\alpha}_P, \omega_P)} \mathbf{x} = -\mathbf{k}^T(\tilde{\alpha}_P, \omega_P) \mathbf{x}. \quad (30)$$

The closed-loop system matrix  $\mathbf{A}_c(\tilde{\alpha}_P, \omega_P)$  depends on the state  $\tilde{\alpha}_P$  as well as the angular velocity  $\omega_P$  and is, hence, not


 Figure 6: State dependent feedback gain  $\underline{k}_{FB}(\mathbf{x})$ .

constant. Its stability is investigated by means of linear matrix inequalities (LMIs), cf. [1], where a common Lyapunov function has to be determined that satisfies the following three inequalities

$$\mathbf{P} > 0, \mathbf{A}_{c,l}^T \mathbf{P} + \mathbf{P} \mathbf{A}_{c,l} < 0, \quad l \in \{1, 2\}, \quad (31)$$

with  $\mathbf{A}_{c,l} = \mathbf{A}_l - \mathbf{b} \mathbf{k}_l^T$ . As a common Lyapunov function has been found by using YALMIP and SeDuMi, see [8, 11], the asymptotic stability of the closed-loop system matrix

$$\mathbf{A}_c(\tilde{\alpha}_P, \omega_P) = \sum_{l=1}^2 h_l(\tilde{\alpha}_P, \omega_P) [\mathbf{A}_l - \mathbf{b} \mathbf{k}_l^T] = \sum_{l=1}^2 h_l(\tilde{\alpha}_P, \omega_P) \mathbf{A}_{c,l} \quad (32)$$

is guaranteed. In a next step, a feedforward control  $u_{FF}$  is derived to achieve steady state accuracy. For a further improvement of the tracking behaviour, a dynamic disturbance rejection is employed. The overall control input is given by

$$u_P = -\mathbf{k}^T(\tilde{\alpha}_P, \omega_P) \mathbf{x} + u_{FF} + u_{DC} \quad (33)$$

and can be calculated as the sum of all three control actions.

### Feedforward Control Design Using Extended Linearisation

For the feedforward control design, the hydraulic torque  $\tau_M$  generated by the hydraulic motor according to (11) is considered as the controlled variable. Thus, the nonlinear output equation is given by (19) and depends on  $\tilde{\alpha}_M$ . The command transfer function can be calculated as

$$G_b(s) = \frac{Y(s)}{U_{FF}(s)} = \mathbf{c}^T(\tilde{\alpha}_M) (s\mathbf{I} - \mathbf{A}_c(\tilde{\alpha}_P, \omega_P))^{-1} \mathbf{b} = \frac{b_0(\tilde{\alpha}_M, \tilde{\alpha}_P, \omega_P)}{N(s)}. \quad (34)$$

Obviously, the numerator of the control transfer function contains no transmission zero. The main idea of the feedforward control design is the modification of the numerator of the control transfer function by introducing a polynomial ansatz for the feedforward control action in the Laplace domain according to

$$U_{FF}(s) = [k_{V0} + k_{V1} \cdot s + k_{V2} \cdot s^2] Y_d(s). \quad (35)$$

For its implementation, the desired trajectory  $y_d(t) = \tau_{M,d}(t)$  as well as the first two time derivatives are available from a state variable filter. The feedforward gains can be computed from a comparison of the corresponding coefficients in the numerator as well as the denominator polynomials of

$$\frac{Y(s)}{Y_d(s)} = \frac{b_0(\tilde{\alpha}_M, \tilde{\alpha}_P, \omega_P) \cdot [k_{V0} + k_{V1} \cdot s + k_{V2} \cdot s^2]}{a_0(\tilde{\alpha}_P, \omega_P) + a_1(\tilde{\alpha}_P, \omega_P) \cdot s + a_2(\tilde{\alpha}_P, \omega_P) \cdot s^2} \quad (36)$$

according to

$$k_{Vi} = \frac{a_i(\tilde{\alpha}_P, \omega_P)}{b_0(\tilde{\alpha}_M, \tilde{\alpha}_P, \omega_P)}, \text{ with } i = 0, 1, 2. \quad (37)$$

The feedforward control is evaluated in the time domain with

$$u_{FF} = k_{V0}(\tilde{\alpha}_M, \tilde{\alpha}_P, \omega_P) \tau_{M,d} + k_{V1}(\tilde{\alpha}_M, \tilde{\alpha}_P, \omega_P) \dot{\tau}_{M,d} + k_{V2}(\tilde{\alpha}_M, \tilde{\alpha}_P, \omega_P) \ddot{\tau}_{M,d}. \quad (38)$$

### Dynamic Disturbance Compensation Using Extended Linearisation

The disturbance  $z$  in (18) depends on the unknown leakage flow  $q_U$ , which has to be estimated, and the states  $\omega_M$  and  $\tilde{\alpha}_M$ . This disturbance has to be compensated to achieve an acceptably small tracking error. The disturbance transfer function from the disturbance input to the controlled output becomes

$$G_e(s) = \frac{Y(s)}{Z(s)} = \mathbf{c}^T(\tilde{\alpha}_M) (s\mathbf{I} - \mathbf{A}_c(\tilde{\alpha}_P, \omega_P))^{-1} \mathbf{e}. \quad (39)$$

Aiming at an ideal disturbance compensation, the following condition has to be fulfilled exactly

$$Y(s) = G_b(s) \cdot U_{DC}(s) + G_e(s) \cdot Z(s) \stackrel{!}{=} 0. \quad (40)$$

As an approximation, an ansatz function  $G_c(s)$  for the dynamic disturbance compensation is introduced according to

$$U_{DC}(s) = G_{DC}(s) \cdot Z(s) = [k_{DC0} + k_{DC1} \cdot s] \cdot Z(s). \quad (41)$$

This ansatz function requires values for the disturbance and its first time derivative. By inserting (41) in (40), the design condition becomes

$$0 \stackrel{!}{=} \underbrace{Z(s)}_{\neq 0} \underbrace{[G_b(s) \cdot G_{DC}(s) + G_e(s)]}_{\stackrel{!}{=} 0}. \quad (42)$$

For an approximate dynamic disturbance compensation, the corresponding ansatz coefficients are chosen in such a way that the first two coefficients in the numerator polynomial vanish. For the evaluation of the dynamic disturbance compensation

$$u_{DC} = k_{DC0}(\tilde{\alpha}_P, \omega_P) z + k_{DC1}(\tilde{\alpha}_P, \omega_P) \dot{z} \quad (43)$$

the required time derivative of the lumped disturbance  $\dot{z}$  is calculated by real differentiation.

## 4. Design of an Extended Kalman Filter

Regarding the state variables of the test rig, see (12), only the difference pressure and the angular velocity of the hydraulic motor are measured, which leads to  $\mathbf{y}_m = [\Delta p \ \omega_M]^T$ . Taking the nonlinearities into account, an extended Kalman Filter (EKF) as a nonlinear version of the well-known Kalman Filter (KF) is designed, cf. [5]. Here, a discrete-time version is envisaged for a combined estimation of the state variables as well as disturbances of the hydrostatic transmission. For this purpose, the state equations (13) are extended by two integrator disturbance models for the disturbance torque as well as the leakage volume flow by

$$\dot{\mathbf{z}}_S = \begin{bmatrix} \dot{q}_u \\ \dot{\tau}_U \end{bmatrix} = \begin{bmatrix} 0 \\ 0 \end{bmatrix}. \quad (44)$$

Then, a discrete-time state-space representation can be calculated by explicit Euler discretisation as follows

$$\begin{aligned}
 \underbrace{\begin{bmatrix} \tilde{\alpha}_{P,k+1} \\ \tilde{\alpha}_{M,k+1} \\ \Delta p_{k+1} \\ \omega_{M,k+1} \\ q_{U,k+1} \\ \tau_{U,k+1} \end{bmatrix}}_{\mathbf{x}_{e,k+1}} &= \underbrace{\begin{bmatrix} \tilde{\alpha}_{P,k} \\ \tilde{\alpha}_{M,k} \\ \Delta p_k \\ \omega_{M,k} \\ q_{U,k} \\ \tau_{U,k} \end{bmatrix}}_{\mathbf{x}_{e,k}} + T_s \underbrace{\begin{bmatrix} -\frac{1}{T_{uP}} \tilde{\alpha}_{P,k} + \frac{k_P}{T_{uP}} u_{P,k} \\ -\frac{1}{T_{uM}} \tilde{\alpha}_{M,k} + \frac{k_M}{T_{uM}} u_{M,k} \\ \left[ \frac{2}{C_H} \bar{V}_P \tan(\alpha_{P,\max} \cdot \tilde{\alpha}_{P,k}) \omega_P - \frac{2}{C_H} \bar{V}_M \sin(\alpha_{M,\max} \cdot \tilde{\alpha}_{M,k}) \omega_{M,k} - \frac{q_{u,k}}{C_H} \right] \\ -\frac{d_V}{J_V} \omega_{M,k} + \frac{\bar{V}_M}{J_V} \sin(\alpha_{M,\max} \cdot \tilde{\alpha}_{M,k}) \Delta p_k - \frac{\tau_{U,k}}{J_V} \\ 0 \\ 0 \end{bmatrix}}_{\boldsymbol{\varphi}_e(\mathbf{x}_{e,k}, \mathbf{u}_k)} + \mathbf{w}, \\
 \underbrace{\begin{bmatrix} \Delta p_k \\ \omega_{M,k} \end{bmatrix}}_{\mathbf{y}_{m,k}} &= \underbrace{\begin{bmatrix} 0 & 0 & 1 & 0 & 0 & 0 \\ 0 & 0 & 0 & 1 & 0 & 0 \end{bmatrix}}_{\mathbf{C}} \mathbf{x}_{e,k} + \mathbf{v}. \tag{45}
 \end{aligned}$$

Here,  $T_s$  stands for the sampling time. The vectors  $\mathbf{x}_{e,k}$  and  $\mathbf{u}_k$  represent the state and input vector at the discrete point of time  $t_k$ , respectively, and the corresponding measured output vector is denoted by  $\mathbf{y}_{m,k}$ . Furthermore, the process noise and the measurement noise are given by  $\mathbf{w}$  and  $\mathbf{v}$ , respectively. Both are assumed to be zero-mean Gaussian white noise processes with zero cross-correlation. The vanishing cross-correlation leads to diagonal covariance matrices  $\mathbf{Q}_{EKF}$  and  $\mathbf{R}_{EKF}$ , characterizing the process noise  $\mathbf{w}$  and the measurement noise  $\mathbf{v}$ .

With the error covariance matrix  $\mathbf{P}_k$ , the algorithm for the discrete-time EKF can be summarized at each time instant  $t_k$  as follows:

- State prediction

$$\tilde{\mathbf{x}}_{e,k+1} = \boldsymbol{\varphi}_e(\hat{\mathbf{x}}_{e,k}, \mathbf{u}_k) \tag{46}$$

- Prediction of the error covariance matrix  $\tilde{\mathbf{P}}_{k+1}$

$$\tilde{\mathbf{P}}_{k+1} = \boldsymbol{\phi}_k \hat{\mathbf{P}}_k \boldsymbol{\phi}_k^T + \mathbf{Q}_{EKF}, \text{ with } \boldsymbol{\phi}_k = \left. \frac{\partial \boldsymbol{\varphi}_e(\mathbf{x}_{e,k}, \mathbf{u}_k)}{\partial \mathbf{x}_{e,k}} \right|_{\mathbf{x}_{e,k} = \hat{\mathbf{x}}_{e,k}} \tag{47}$$

- Update of the gain matrix  $\tilde{\mathbf{L}}_{k+1}$

$$\tilde{\mathbf{L}}_{k+1} = \tilde{\mathbf{P}}_{k+1} \mathbf{C}^T (\mathbf{C} \tilde{\mathbf{P}}_{k+1} \mathbf{C}^T + \mathbf{R}_{EKF})^{-1} \tag{48}$$

- Update of the state vector  $\hat{\mathbf{x}}_{e,k+1}$

$$\hat{\mathbf{x}}_{e,k+1} = \tilde{\mathbf{x}}_{e,k+1} + \tilde{\mathbf{L}}_{k+1} (\mathbf{y}_{m,k+1} - \mathbf{C} \tilde{\mathbf{x}}_{e,k+1}) \tag{49}$$

- Update of the error covariance matrix for the next sampling interval

$$\hat{\mathbf{P}}_{k+1} = (\mathbf{I} - \tilde{\mathbf{L}}_{k+1} \mathbf{C}) \tilde{\mathbf{P}}_{k+1} \tag{50}$$

## 5. Simulation Results

In this section, a simulation study of the proposed decentralized nonlinear control for the hydrostatic transmission in combination with the extended Kalman Filter is described. The implemented control structure is depicted in Fig. 7. To obtain a realistic simulation, the simulated leakage flow is assumed to be proportional to the pressure difference according to

$$q_U = 1 \cdot 10^{-12} \Delta p, \tag{51}$$

whereas the simulated disturbance torque is given by

$$\tau_U = 0.1 J_V \dot{\omega}_M + 7 \tanh\left(\frac{\omega_M}{0.1}\right). \tag{52}$$

The trajectory of the variable angular velocity  $\omega_P$  of the drive motor is depicted in Fig. 8. In addition to the disturbance models, measurement noise is added in the simulations to the difference pressure  $\Delta p$  and the motor angular velocity  $\omega_M$ , which are the only measurable state variables at the test rig.

The obtained results from the simulation are depicted in the following figures. The high tracking performance of  $\tilde{\alpha}_M$  is visible in Fig. 9. In Fig. 10, the simulation results of hydraulic motor torque are presented, which match well. According to the equation of motion of the hydraulic motor, the angular velocity  $\omega_M$  follows as shown Fig. 11a. The obtained difference pressure is depicted in the Fig. 11b.

The next figures point out the benefits of the disturbance estimation by the extended Kalman Filter. The simulated disturbance torque  $\tau_U$  as well as the estimate  $\hat{\tau}_U$  are shown in Fig. 12a. It becomes obvious that the EKF is capable of accurately reconstructing this unknown disturbance. The same holds for the other disturbance, the leakage flow  $q_U$ , which is depicted in Fig. 12b.

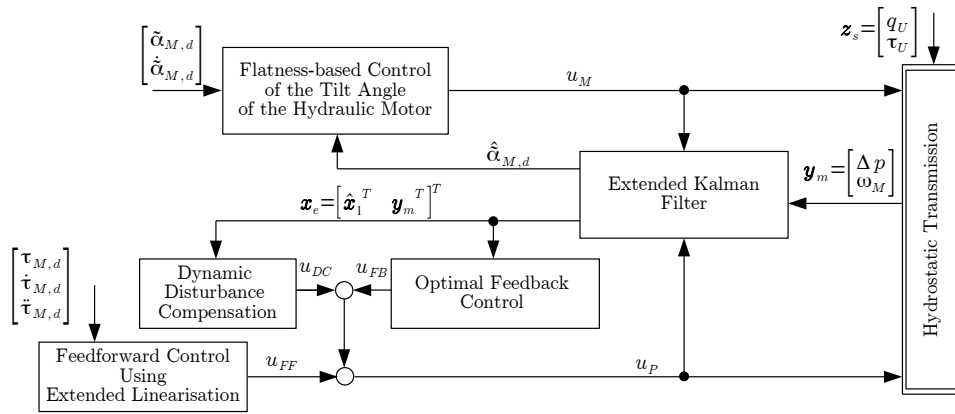
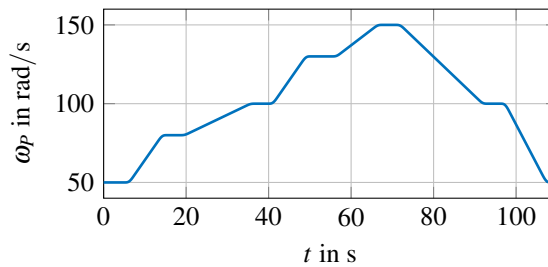


Figure 7: Block diagram of the implemented control structure.

Figure 8: Trajectory of the adapted angular velocity of the drive motor  $\omega_p$ .

## 6. Conclusions

An innovative decentralized nonlinear control design is proposed for a hydrostatic transmission. For the hydraulic motor torque of the hydrostatic transmission, an optimal tracking control is derived using Takagi-Sugeno techniques, whereas the control of normalized tilt angle of the hydraulic motor is realized by a flatness-based approach. Moreover, an extended Kalman Filter is introduced to accurately estimate unmeasurable system states and unknown disturbances. The control performance of the proposed control structure is shown by simulation results using a validated system model of a test rig at the Chair of Mechatronics, University of Rostock.

## References

- [1] Boyd, S., Ghaoui, L.E., Feron, E., and Balakrishnan, V.: Linear Matrix Inequalities in System and Control Theory, 1994, SIAM.
- [2] Dolan, B., and Aschemann, H.: Control of a Wind Turbine with a Hydrostatic Transmission - An Extended Linearisation Approach. In *17th International Conference on Methods and Models in Automation and Robotics (MMAR)*, 2012, pp. 445–450.
- [3] Diepeveen, N.F.B., and Laguna, A.J.: Dynamics Modelling of Fluid Power Transmissions for Wind Turbine In *EWEA Offshore*, 2011, Amsterdam, Netherland.
- [4] Fliess, M., Levine, J., Martin, P. and Rouchon, P.: Flatness and Defect of Nonlinear Systems: Introductory Theory and Examples. In *Int. J. Control*, 1995, vol. 61, pp=1327–1361.
- [5] Friedland, B.: Advanced Control System Design, 1996, Prentice Hall.
- [6] Jelali, M. and Kroll, A.: Hydraulic Servo Systems: Modelling, Identification and Control, 2003, Springer.
- [7] Prabel, R. and Aschemann, H.: Torque Control of a Hydrostatic Transmission Using Extended Linearisation Techniques. In *Scandinavian Intern. Conf. on Fluid Power (SICFP)*, 2017, Linköping, Sweden.
- [8] Löfberg, J.: YALMIP: A Toolbox for Modelling and Optimization in MATLAB. In *Symp. on Computer Aided Control Systems Design*, 2004, pp. 284–289.
- [9] Schulte, H., and Gerland, P.: Control-Oriented Modeling of Hydrostatic Power-Split CVTs Using Takagi-Sugeno Fuzzy Models. In *7th Conference of the European Society for Fuzzy Logic and Technology (EUSFLAT)*, 2011, pp. 797–804.
- [10] Schulte, H.: Control-Oriented Description of Large Scale Wind Turbines with Hydrostatic Transmission Using Takagi-Sugeno Models. In *Conference on Control Applications (CCA)*, 2014, Antibes, France.
- [11] Sturm, J.F.: Using SeDuMi 1.02, A Matlab Toolbox for Optimization Over Symmetric Cones, In *Optimization Methods and Software*, 1999, no. 11-12, pp. 625–653.
- [12] Sun, H., and Aschemann, H.: Quasi-Continuous Sliding Mode Control Applied to a Hydrostatic Transmission. In *European Control Conference (ECC)*, 2015, Linz, Austria.
- [13] Sun, H., Prabel, R., and Aschemann, H.: Cascaded Control Design for the Tracking Control of a Hydrostatic Transmission Based on a Sliding Mode State and Disturbance Observer. In *Conf. on Methods and Models in Automation and Robotics (MMAR)*, 2016, pp. 432–437.
- [14] Tanaka, K. and Wang, H.O.: Fuzzy Control Systems Design and Analysis: A Linear Matrix Inequality Approach, 2001, Wiley.

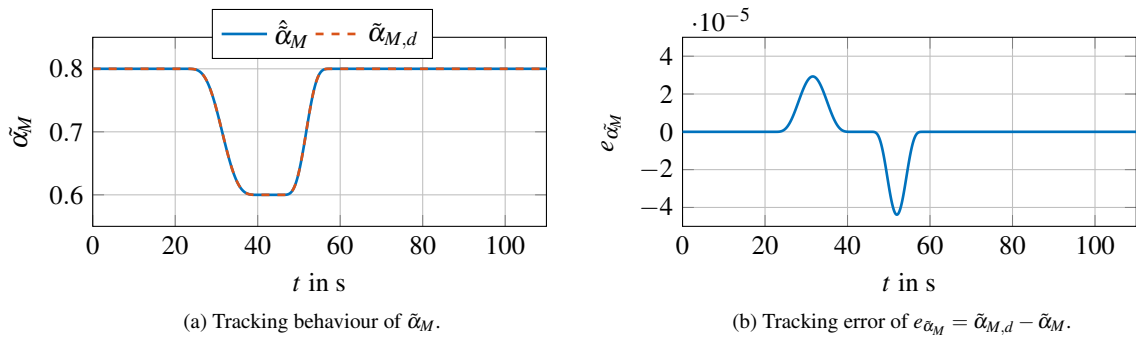


Figure 9: Tracking behaviour of tilt angle of the hydraulic motor  $\tilde{\alpha}_M$ .

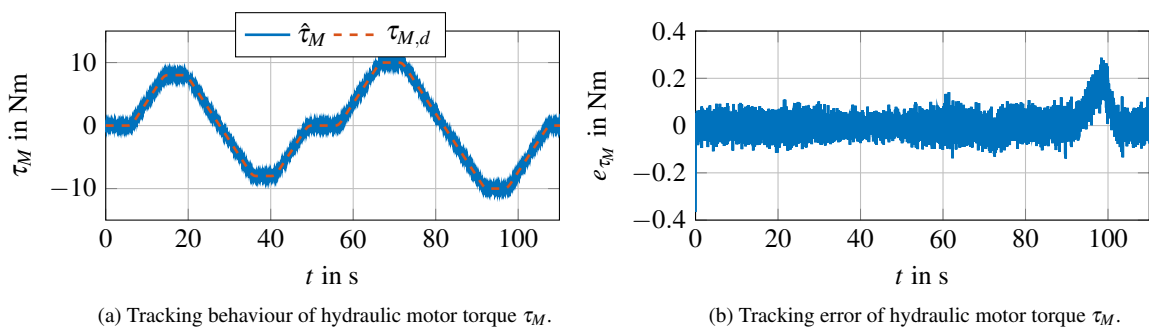


Figure 10: Tracking behaviour of the hydraulic motor torque.

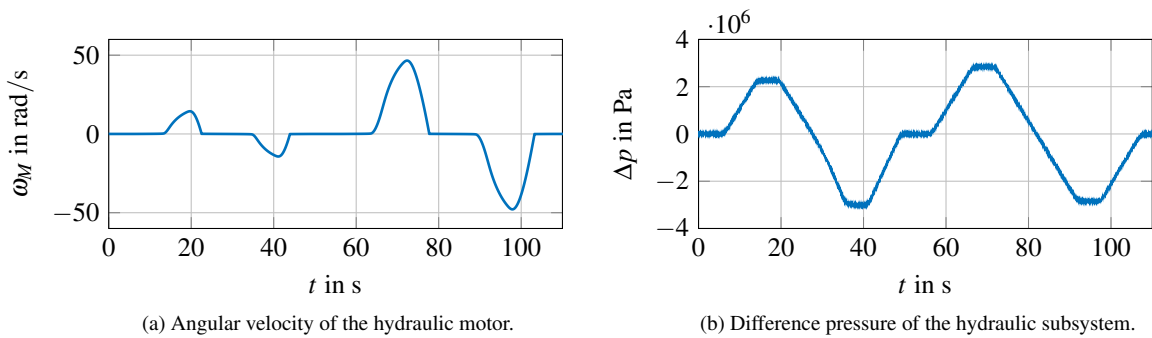


Figure 11: Remaining states (simulation results).

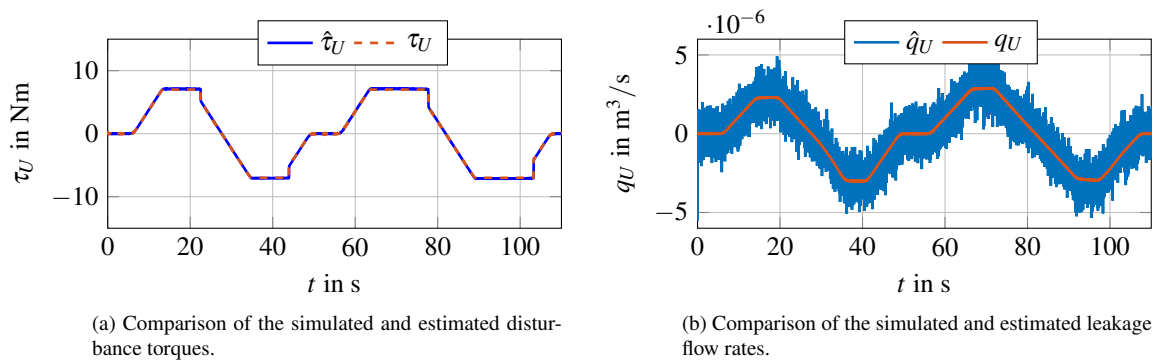


Figure 12: Comparison of the simulated and estimated disturbances.